

Penck1D: Transport- and production-limited fault scarp simulation software

George E. Hilley
Institut für Geowissenschaften
Universität Potsdam
14415 Potsdam, Germany

J Ramón Arrowsmith
Department of Geological Sciences
Arizona State University
Tempe, AZ 85287-1404

Contents

1	Introduction	5
2	Tectonic deformation and geomorphic transport of regolith	7
2.1	Observations of alluvial and bedrock scarps	7
2.2	Conceptual and numerical model of scarp degradation	9
2.2.1	Tectonic processes	9
2.2.2	Geomorphic processes	11
2.2.3	Coupled tectonic and geomorphic model	12
3	Solution by Finite Difference Method (FDM)	15
3.1	Introduction	15
3.2	Diffusive Hillslope Transport	15
3.2.1	Review of basic derivation	15
3.2.2	Analytical solutions to the diffusion equation–Vertical scarp initial conditions	16
3.2.3	Analytical solutions to the diffusion equation–Finite slope scarp initial conditions	16
3.2.4	Analytical solutions to the diffusion equation–repeated faulting	17
3.3	Finite difference approximation	18
3.3.1	Taylor series and approximations of the first derivative	18
3.3.2	Finite difference approximations of higher order derivatives	19
3.4	Numerical solutions to the basic linear diffusion erosion problem	20
3.4.1	Derivation	20
3.4.2	Benchmarking the method–how accurate is it?	21
3.4.3	An example application of the 1-D explicit finite difference method solved using a spreadsheet (Microsoft Excel)	21
4	How to use the software	25
4.1	Introduction	25
4.2	Using the program	25
4.2.1	A note about units	25
4.2.2	Starting the program	25
4.2.3	General model building procedure	25
4.2.4	Setting model parameters	26

4.2.5	Menu functions	29
4.3	Examples of fault scarp simulation	35
4.3.1	Example 1: Flat initial topography offset by reverse faulting	35
4.3.2	Example 2: Sloping initial topography offset by normal faulting	37
4.3.3	Example 3: Measured initial topography (imported data) offset by normal faulting . .	39
5	Final Thoughts: Validity of scarp modeling approach	41

Chapter 1

Introduction

This manual provides a general introduction to numerical scarp modeling, including the principles of tectonic and geomorphic transport, a description of the basics of the numerical method used to solve the transport equations, and a how-to guide for using the Penck1D graphical software in Matlab. The manual is organized into three basic parts: an overview of the principal observations of regolith mantled and bedrock scarps (Chapter 2), the solution of the equations of displacements and diffusive geomorphic transport using the Finite Difference Method (Chapter 3), and a how-to manual for using the software (Chapter 4). Finally, we provide a brief discussion of the applications of the fault scarp modeling approach, its validity, and areas of future research in this subject.

If you use Penck1D in your research, please acknowledge this document and the software development documents as follows:

Hilley, G. E., and J R. Arrowsmith, 2001, Penck1D: Transport- and production- limited fault scarp simulation software, GSA Special Short Course Manual, 44 p.

Hilley, G. E., 2001, Landscape development in tectonically active mountain belts using geologic and geomorphic observations, digital topography analysis, and numerical models, Ph.D. dissertation, Arizona State University, 194 p.

In addition, please report any bugs to George Hilley at hilley@geo.uni-potsdam.de. Please send a reprint of any publications to George Hilley (current address available through email request). Finally, please feel free to improve upon the model and add features, but be sure to send me a copy of the improved software so that I can post these improvements on the web for general use.

Chapter 2

Tectonic deformation and geomorphic transport of regolith

2.1 Observations of alluvial and bedrock scarps

A fault scarp is a tectonic landform where the fault plane, or a zone of interconnected fault segments, intersects the land surface [Stewart and Hancock, 1990]. Fault scarps may be formed by offset of regolith or bedrock. When bedrock is not exposed, the amount of sediment available for transport is larger than the transport capacity of the geomorphic processes, and hence the scarp is transport-limited. However, once bedrock is exposed, there may be excess transport capacity relative to the amount of transportable sediment. In these cases, sediment cannot be transported until it is produced by bedrock weathering. Thus, bedrock scarps are production-limited [Carson and Kirkby, 1972]. The morphology of transport-limited scarps is controlled primarily by the rate at which material can be transported, whereas production limited scarp morphology is controlled by the production rate of transportable material from bedrock.

The morphology of transport- and production-limited scarps is often markedly different (Figure 2.1a and b). Fresh transport-limited scarps show a steep face that is often dominated by mass failure, and sometimes gullying. Usually these slopes are reduced to the internal angle of friction of the material soon after rupture [Figure 2.1a; *e.g.*, McCalpin, 1996]. This transport results in the deposition of colluvium at the base of the scarp as the upper edge is bevelled (Figure 2.2a). Following degradation of the scarp by mass failure, material in channels and gullies is transported by fluvial processes, whereas local hillslope processes transport material across the scarp in the interfluvies (Figure 2.2a). Where gullying and channelization are not significant, the scarp typically shows a smooth profile, with a convex-up form on the upper part of the scarp and a concave-up form on the lower slopes of the scarp [*e.g.*, Nash, 1980; Figure 2.1b). As faulting continues, the scarp elevation and curvature is increased and the process is started anew.

Production-limited scarps do not display the smooth morphology typical of transport-limited scarps (Figure 2.1c and d). These fault scarps are often expressed as bedrock cliffs that may show structural kinematic indicators of motion along the fault. With time, the bedrock face of the scarp is converted to regolith that is transported downslope into the colluvial pile at the base of the scarp (Figure 2.2b). Material may also be transported to the base of the scarp by gravity failure along pre-existing mechanical weaknesses such as fractures. In this process, rock topple and mass failure may act to degrade the scarp. Where these processes are not significant, the scarp can retain its steepness for long periods of time in places where the production rate of transportable regolith from bedrock is low. Further movement along the fault acts to increase the height of the bedrock scarp face. The isolation of transportable material at the top of the scarp from the bottom may prevent slope steepening at the scarp face from accelerating the amount of sediment moving to the base of the scarp. However, after sufficient time, the scarp is degraded as the bedrock is converted to regolith and transported away from the high-slope areas.

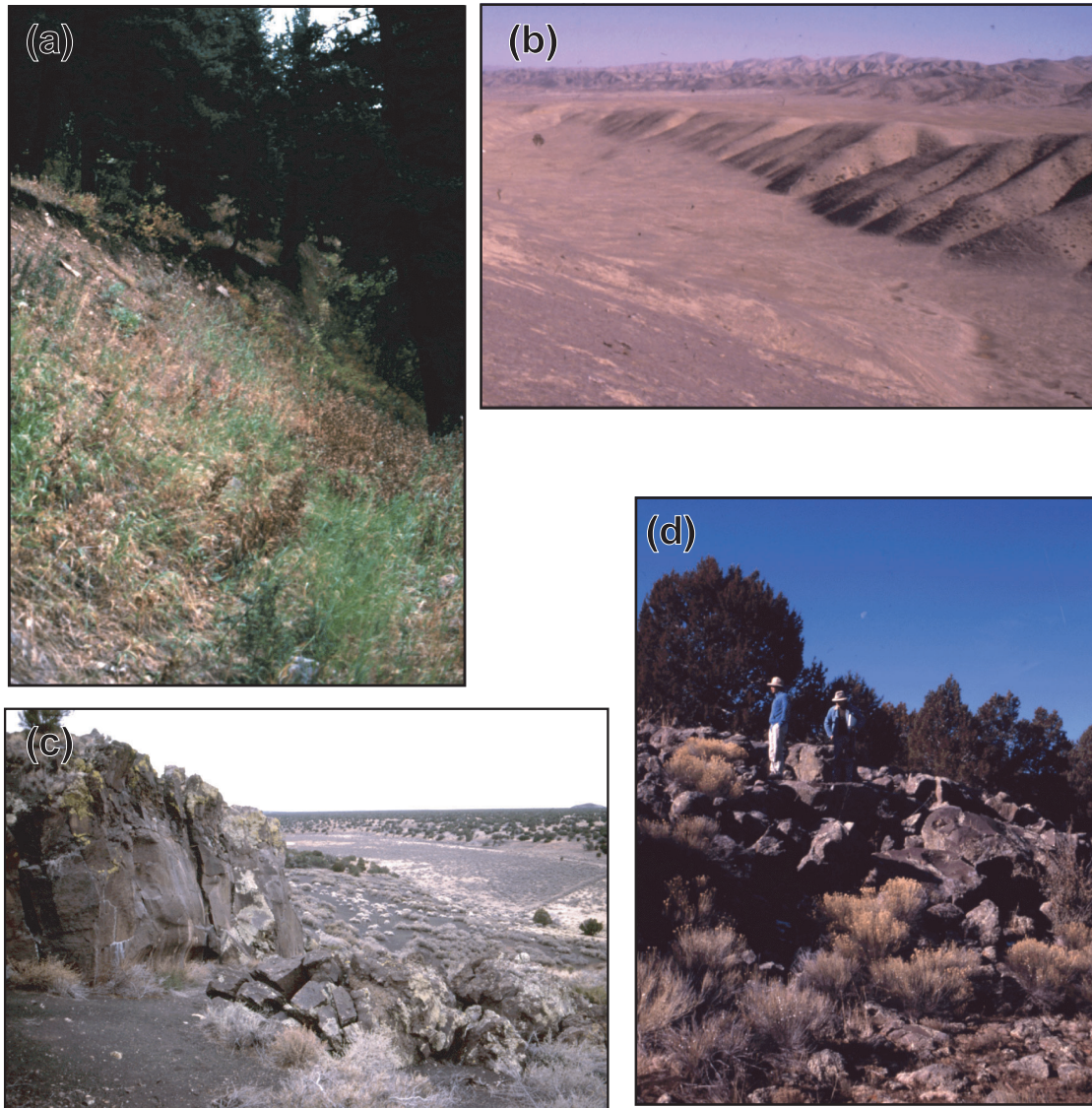


Figure 2.1: Degradation of transport-limited (a)–(b) and production-limited (c)–(d) scarps. (a) Following rupture, transport-limited scarps form a steep linear profile whose angle is typically close to the angle of repose of the material. (b) With time, geomorphic processes bevel the upper edge of the scarp and deposit this material at its base. We consider in our analysis only those areas of the scarp located in the interfluvies. (c) In contrast, rupture along production-limited faults exposes bedrock, creating a bedrock cliff. (d) After movement along the fault ceases, the bedrock scarp degrades, reducing the scarp slopes. Photos taken at (a) the Hebgen Lake fault scarp, MT (Cabin Creek locality) (b) a normal fault in the Carrizo Plain, CA, (c) Della Tank graben, and (d) Babbitt Lake fault scarp, both in northern Arizona.

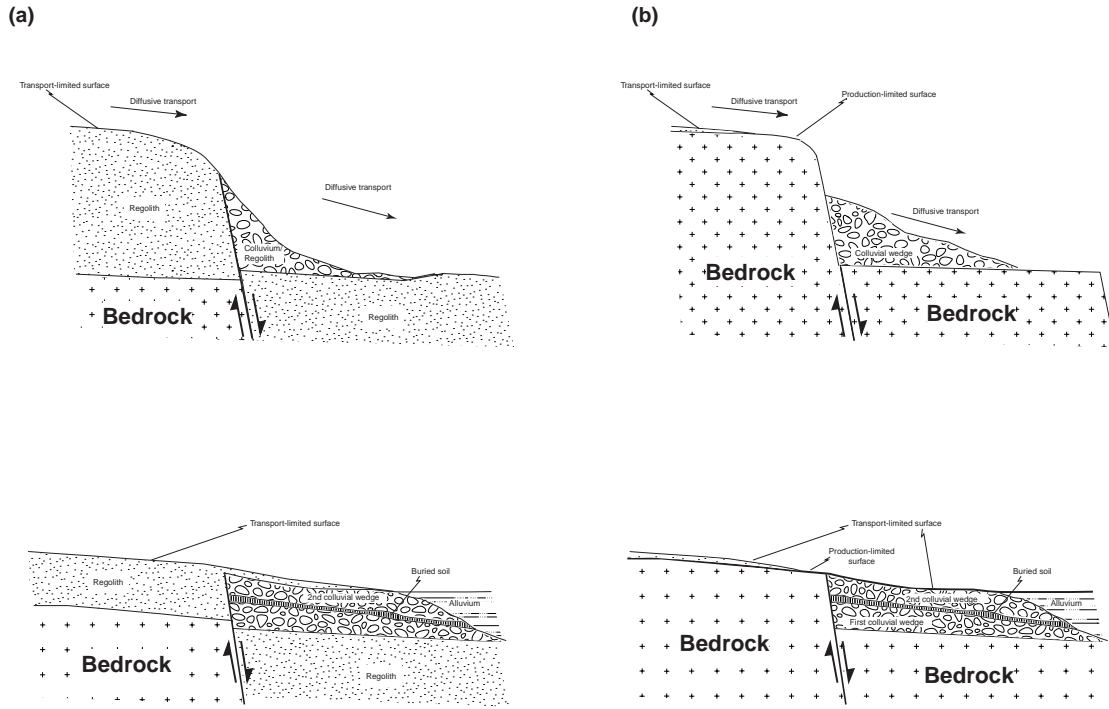


Figure 2.2: Schematic figure showing the development of (a) transport- and (b) production-limited scarps. Topography and depositional patterns emphasize near-fault development. The lower figures show the development of the scarp after significant time has passed.

2.2 Conceptual and numerical model of scarp degradation

To understand how active faults may be morphologically expressed, we built a model that relates the topography to the tectonic and geomorphic processes that form fault scarps. Our general approach couples constitutive equations that characterize tectonic deformation and geomorphic processes to the equations of continuity (mass conservation) to numerically model scarp development over time. We limit our analysis to the consideration of systems in which there are neither displacements nor geomorphic transport in the out-of-plane dimension of a topographic profile of the scarp. This reduces the model to a one-dimensional geomorphic transport model that is displaced by two-dimensional tectonic displacements.

2.2.1 Tectonic processes

In our tectonic model, we assume that the upper crust can be approximated by a brittle linear-elastic rheology that deforms in response to slip along and opening of discontinuities in the medium. We model fault-induced surface displacements by embedding a dislocation in an elastic half-space and letting it slip a prescribed amount. The geometry of the fault can be expressed by two parameters—the fault dip, β , and the down dip length of the fault surface, W . We assume that the fault is infinitely long in the out-of-plane dimension, and hence, deformation is approximated by plane-strain conditions (Figure 2.3a). The slip along the fault is described by the Burgers vector (b). Positive and negative Burgers vectors on faults dipping to the right indicates reverse and normal motion along the fault, respectively.

Given these three parameters, the surface displacements can be computed by summing the effects of two opposing, infinitely long edge dislocations starting at the upper (w_1 in Figure 2.3a) and lower (w_2 in Figure 2.3a) edges of the fault, respectively. The equations for relating surface displacements to fault geometric parameters are [Du *et al.*, 1994]:

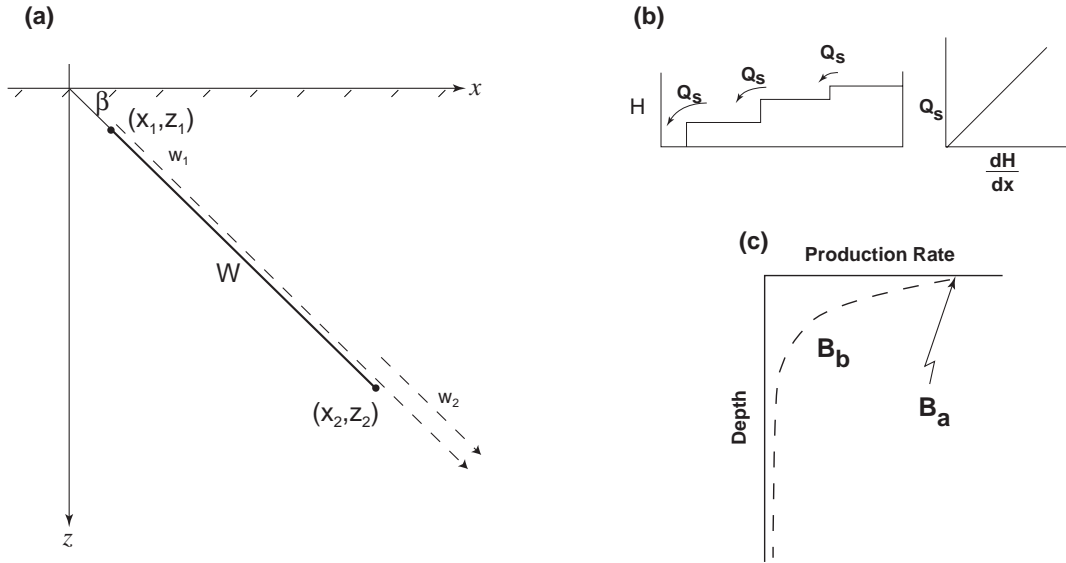


Figure 2.3: Model fault geometry and controlling parameters. (a) The surface displacements are computed by summing the effect of slip along two infinite dislocations extending downward (w_1 , w_2), whose ends start at (x_1, y_1) and (x_2, y_2) , respectively. The hachured line is the free surface and the solid line is the idealized fault. (b) The volume flux of sediment (Q_s) moved downhill by geomorphic processes is proportional to the local slope. Changes in elevation with time due to changes in Q_s downslope are computed numerically. (c) Regolith is produced from bedrock as an exponential function of regolith thickness. Production is maximum at the surface (B_a) and decays according to the regolith thickness sensitivity, B_b .

$$U_x = -\frac{1}{\pi} \left(b_x \tan^{-1}(d) + \frac{b_z - b_x d}{1 + d^2} \right) \quad (2.1)$$

$$U_z = \frac{1}{\pi} \left(b_z \tan^{-1}(d) + \frac{b_x + b_z d}{1 + d^2} \right) \quad (2.2)$$

where, U_x is the horizontal displacement at the free surface (L),
 U_z is the vertical displacement at the free surface (L),
 b_x is the horizontal component of the Burgers vector (L),
 b_z is the vertical component of the Burgers vector (L),
and d is the geometric parameter.

The geometric parameter locates the tip of the dislocation relative to the point of interest along the free surface:

$$d = \frac{(x - x_n)}{z_n} \quad (2.3)$$

where x is the horizontal coordinate of the surface point of interest (L),
 x_n is the x coordinate of the tip of the n^{th} dislocation (L),
 and z_n is the vertical coordinate of the tip of the n^{th} dislocation (L).

Finally, the dip of the dislocation is defined by the magnitudes of the components of the Burgers vectors. The components of the Burgers vector are related to the fault dip as, $b_x = b \cos \beta$ and $b_z = b \sin \beta$.

Surface displacements are determined by summing the displacements U_x and U_z due to the two oppositely oriented dislocations defining the slip patch. By repeating this calculation for many points along the surface, we can determine the surface displacement field due to slip along the simulated fault. Although these equations relate fault slip to surface displacement, they may also be used to compute surface displacement rates by differentiating Equations 2.1 and 2.2 with respect to time.

2.2.2 Geomorphic processes

Geomorphic transport

Where channels, landsliding, aeolian transport, and glacial processes do not exist, the geomorphic surface sediment transport rate is approximately proportional to the local slope angle [e.g., *Davis*, 1892; *Gilbert*, 1909; *Culling*, 1960; *Koons*, 1989; *McKean et al.*, 1993; *Small et al.*, 1999]. First, we use a linear diffusive transport law that approximates the effects of bioturbation, rain splash, and sheet wash [e.g., *Carson and Kirkby*, 1972]. In this formulation, the flux of material through a point along an unchannelized hillslope is proportional to the local slope (Figure 2.3b):

$$Q_s = -\kappa \frac{dH}{dx} \quad (2.4)$$

where, Q_s is the volume flux of material moving through a point (L^2/T),
 κ is the hillslope diffusivity (L^2/T),
 and H is the topographic elevation (L).

Next, continuity along the profile (mass conservation) requires that the change in the mass at each point in a small amount of time is equal to the difference in the mass flux (Q_m) entering and leaving that point:

$$\frac{\partial m}{\partial t} = \frac{dQ_m}{dx} = \frac{d(Q_s \rho_s(x, y, t))}{dx} \quad (2.5)$$

Assuming that the density of sediment does not significantly change during transport, this mass flux can be rewritten as the volume flux:

$$\frac{\partial H}{\partial t} = \frac{dQ_s}{dx} \quad (2.6)$$

By combining Equations 2.4 and 2.6, we can express the change in elevation over time at a point in terms of the hillslope curvature:

$$\frac{\partial H}{\partial t} = -\kappa \nabla^2 H \quad (2.7)$$

The hillslope diffusivity, κ has been determined to be between 0.04 and 0.0004 m²/yr [Fernandes and Dietrich, 1994, and references therein; Hanks, 2000] and may vary with climate, aspect, density of vegetation, and other factors [e.g., Hanks, 2000].

Transport of material can only take place when there is sufficient sediment to transport. In the case that $\partial H/\partial t$ exceeds the thickness of transportable material over a given time increment, there is excess transport capacity of the system relative to the available sediment. Therefore, the transport process erodes all sediment available for transport, but fails to transport at full capacity. In the case that the transport capacity exceeds available material, the flux of material moving downslope at points where these production-limited conditions exist are computed by transporting only material that is available, $H - B$ (where B is the elevation of the bedrock (L)) and recomputing the fluxes along the scarp:

$$Q_s(x, y) = \frac{H(x, y, t) - B(x, y, t)}{\partial t} \partial x \quad (2.8)$$

We iteratively recompute all fluxes to calculate the change in elevation across parts of the landscape that may be either transport- or production-limited.

Regolith production from bedrock

In general, it is assumed that bedrock is converted to regolith at a rate that decreases with increasing regolith thickness [Ahnert, 1970; Carson and Kirkby, 1972; Heimsath et al., 1998; Heimsath et al., 1999; Small et al., 1999]. This rate is thought to decay either exponentially [e.g., Heimsath et al., 1998; Heimsath et al., 1999; Carson and Kirkby, 1972; Ahnert, 1970; Anderson and Humphrey, 1989] or as a ζ -function [Ahnert, 1970; Carson and Kirkby, 1972]. The simple transport law and regolith production function constitute the process rules in our geomorphic model. In the simple case that production rate decreases with increasing regolith thickness, production at a given depth is described by the surface production rate, B_a , the thickness sensitivity, B_b , and the regolith thickness, $H - B$ (Figure 2.3c):

$$\frac{\partial B}{\partial t} = -B_a e^{-B_b(H-B)} \quad (2.9)$$

where, B_a is the production rate of regolith when bedrock is exposed (L/T),
and B_b is the thickness sensitivity of production rates (1/L).

In this formulation, the production rate of transportable material is largest when the bedrock is exposed and decreases as the thickness of transportable material increases. Larger surface production rates result in faster conversion of bedrock to regolith along the entire profile, whereas smaller values of the thickness sensitivity allow production rates to remain larger with depth than do large values of B_b . Measurements using cosmogenically produced ²⁶Al and ¹⁰Be by Heimsath et al. [1998] along study sites in the northern Bay Area, California and Coast Ranges, Oregon, indicate $B_a = 8 \times 10^{-5}$ m/yr and $B_b = 2$ m⁻¹.

2.2.3 Coupled tectonic and geomorphic model

We combined these models of tectonic deformation, geomorphic transport, and production of regolith from bedrock to understand the influence of various processes and rates on the morphologic development of scarps. We reduced our geomorphic transport and tectonic models to a one-dimensional system by assuming that all transport takes place along a cross-section (*i.e.*, there is no out of plane movement of material). This represents an infinitely long scarp perpendicular to the geomorphic transport direction. While the tectonic displacement rates may be computed directly, we solved the geomorphic transport and regolith production

equations by finite differences [*e.g.*, *Ferziger*, 1981]. In this numerical method, the solution domain is divided into regularly spaced elements. Elevation profiles are numerically differentiated twice in space and integrated once in time to compute the change in the profile over a certain time increment, Δt , using prescribed boundary conditions. With each successive time step, we add the appropriate tectonic displacements and produce additional regolith according to our tectonic and regolith production laws. In the model, the fault may slip in discrete events or continuously. If the fault slips discretely, displacements resulting from the characteristic fault slip are added to the profile length (x) and elevation values (H) when the model time since the last rupture exceeds the recurrence time of the fault. In the case of a continuously slipping fault, displacements are added during each time step of the model. We reinterpolate the surface elevations at each successive time step and allow node overlap of the bedrock profile to simulate faulting of bedrock against regolith. We used a second and first order differentiation and integration method, respectively, to solve the discrete partial differential equations. To ensure numerical stability and accuracy of the solution, we used time-steps two orders of magnitude lower than those required by the one-dimensional diffusive stability criterion ($\Delta t = 0.01 \times \partial x^2 / 2\kappa$). In all of our models, we assume an initially flat topography and bedrock/regolith interface at $t = 0$. In order to accommodate production-limited conditions, we adjusted the downslope flux where bedrock was exposed according to the thickness of available transportable material. The adjusted elevation change is then added to the profile elevation for each successive time step until the end of the model duration. In all transport-limited models, constant elevation boundary conditions far from the fault are used where induced displacements are effectively zero. In our production-limited models, we allowed the left and right boundaries to change their elevations as they are displaced by fault movement.

Chapter 3

Solution by Finite Difference Method (FDM)

3.1 Introduction

Intuition about the relationship between tectonic and geomorphic processes and the resulting topography may be built by combining detailed field observations with careful theoretical analysis. While detailed observations are commonly the cornerstone of sound geologic studies, theoretical modelling of the processes involved that produce the observations is often impaired by the inability to solve the governing equations of these processes for typical geologic conditions. However, numerical methods may be employed that let us approximate the governing differential equations for a wide range of geologically applicable scenarios.

This section describes and illustrates a simple implementation of the Finite Difference Method (FDM) for investigating the development of hillslope topography. Using this numerical technique, we show how simple ideas about the transport of geomorphic material, production of regolith from bedrock, and relative tectonic displacements may be used to extrapolate limited observations of topography at a particular time to approximations of how the topography might have looked in the past and future. In addition, conceptual models, cast in the language of mathematics, allow us to link observations that typically do not directly tell us about the underlying processes to the processes themselves. This portion of the document is modified from *Arrowsmith* [1995].

3.2 Diffusive Hillslope Transport

3.2.1 Review of basic derivation

We use for our example of the finite difference method a hillslope whose transport is governed only by the local slope and some transport constant and for which conditions are transport-limited. This situation is described in a previous section, and results in the following governing differential equation for material transport:

$$Q(x) = -\kappa \frac{\partial H}{\partial x} \quad (3.1)$$

Where x is the location of each point along the profile [L], H is the elevation at that point [L], κ is the hillslope diffusivity (rate constant in eq. 3.1[L²], and $Q(x)$ is the flux of material per unit width at each point [L²].

In addition, if the density of sediment remains constant during transport, any change in flux must be compensated by either 1) the addition or removal of material at each point, or 2) a change in the elevation. This mass balance can be expressed in the form of the continuity equation:

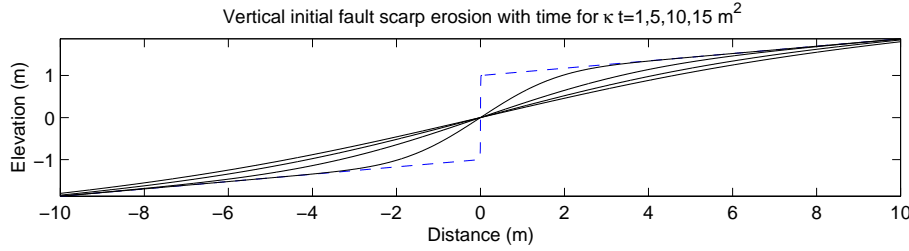


Figure 3.1: The geometry of a simple initially vertical fault scarp and its subsequent degradation with time (morphologic ages of 1, 5, 10, and 15 m^2). Dashed line is the initially vertical profile, the initial offset ($2a$) is 2 m, and $b = 5^\circ$.

$$\frac{\partial H}{\partial t} = -\frac{\partial Q}{\partial x} \quad (3.2)$$

These two equations constitute the constitutive equations of diffusive hillslope erosion. Substitute the transport rule (eq. 3.1) for $Q(x)$ into the continuity equation (eq. 3.2) to get the homogeneous linear diffusion equation in which the change in elevation with time is proportional to the local curvature of the topographic profile:

$$\frac{\partial H}{\partial t} = \kappa \frac{\partial^2 H}{\partial x^2} \quad (3.3)$$

Eq. 3.3 is analogous to the heat conduction equation for one dimensional heat transport in which κ would be the coefficient of proportionality called the thermal conductivity and H would be temperature (e.g., Avouac, 1993; Hanks et al., 1984; Nash, 1980).

3.2.2 Analytical solutions to the diffusion equation—Vertical scarp initial conditions

First, we will illustrate the analytic solutions to the simple diffusion equation (an approach presented in Hanks et al., 1984). A solution of the homogeneous linear diffusion equation (eq. 3.3) for a step of topography of $2a$ at $t = 0$ and $x = 0$ (e.g., a newly formed fault scarp, and note that the origin for x in this example is in the midscarp and not at the upper boundary) on a pre-existing topographic slope of b is

$$H(x, t) = a \operatorname{erf}\left(\frac{x}{2\sqrt{\kappa t}}\right) + bx \quad (3.4)$$

The resulting profiles are not uniquely dependent on t or κ , but rather their product. For example, the same profile will result for $\kappa = 1 \text{ m}^2/\text{kyr}$ and $t = 10 \text{ kyr}$ or $\kappa = 10 \text{ m}^2/\text{kyr}$ and $t = 1 \text{ kyr}$. (*T. C. Hanks personal communication* and Hanks et al., 1984). For this presentation, we have separated these values to emphasize the fact that a known value for κ or t may be used to constrain the other. Figure 3.1 shows the geometry of this simple fault scarp and a graphical solution to 3.4 for a step of 2 m at time zero and a far field or fan slope of 5° , and its subsequent degradation with time.

3.2.3 Analytical solutions to the diffusion equation—Finite slope scarp initial conditions

Equation 3.4 provided a solution of the diffusion equation (eq. 3.3) for an infinite slope (vertical) initial scarp slope (Figure 3.1). Clearly, a vertical scarp will not last long, nor will “diffusive” processes operate on such steep slopes. Therefore, it is important to develop the analysis for finite initial slope scarps. Hanks

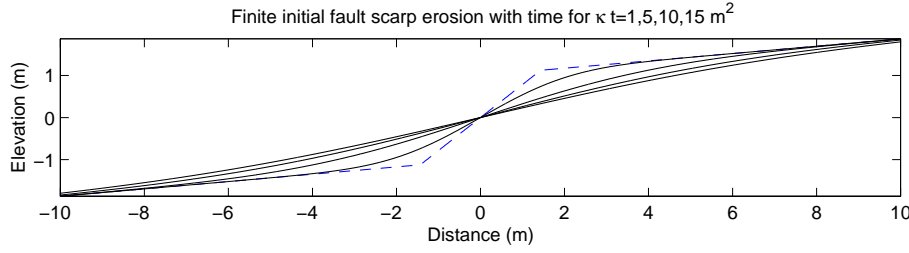


Figure 3.2: The geometry of a finite initial slope fault scarp and its subsequent degradation with time (morphologic ages of 1, 5, 10, and 15 m^2). Dashed line is the initial profile (initial scarp slope of 45°), the initial offset ($2a$) is 2 m, and $b = 5^\circ$.

and Andrews (1989) provided the following equation for the same conditions that give rise to eq. 3.4, except that the rupture “occurs” on a slope of θ instead of ∞ . The solution to eq. 3.3 is:

$$\begin{aligned}
 H(x, t) = & (\theta - b) \left(\frac{\kappa t}{\pi} \right)^{1/2} \left\{ \exp \left(-\frac{x + a/(\theta - b)}{4\kappa t} \right)^2 - \exp \left(-\frac{x - a/(\theta - b)}{4\kappa t} \right)^2 \right\} \\
 & + \frac{\theta - b}{2} \left\{ \left(x + \frac{a}{\theta - b} \right) \operatorname{erf} \left(\frac{x + a/(\theta - b)}{(4\kappa t)^{1/2}} \right) - \left(x - \frac{a}{\theta - b} \right) \operatorname{erf} \left(\frac{x - a/(\theta - b)}{(4\kappa t)^{1/2}} \right) \right\} \\
 & + bx
 \end{aligned} \tag{3.5}$$

Figure 3.2 shows the geometry of this simple fault scarp and a graphical solution to 3.5 for a step of 2 m at time zero and a far field or fan slope of 5° , and a finite initial scarp slope of 45° , and its subsequent degradation with time.

3.2.4 Analytical solutions to the diffusion equation—repeated faulting

For the case of a constant offset in the middle of the profile (instantaneously vertical), the solution to eq.3.3 for a slip rate $2A$ with initial scarp offset $2a$ is:

$$\begin{aligned}
 H(x, t) = & (a + At) \operatorname{erf} \left(\frac{x}{2\sqrt{\kappa t}} \right) \\
 & + \left\{ \left(\frac{Ax^2}{2k} \right) \operatorname{erf} \left(\frac{x}{2\sqrt{\kappa t}} \right) - \operatorname{sgn} x \right\} \\
 & + \left\{ \left(\frac{Ax}{2k} \right) \sqrt{\frac{\kappa t}{\pi}} \exp \left(-\frac{x^2}{4\kappa t} \right) \right\} + bx
 \end{aligned} \tag{3.6}$$

The *MATLAB* codes for solving these equations are available at <http://activetectonics.la.asu.edu/diffuse/>

For some specific initial and boundary conditions, analytic solutions such as those presented in this and the last section may be solved [e.g., Carslaw and Jaeger, 1959 and see Hanks, 2000 and references therein]. However, in many geologic environments, initial profiles may be complicated. Also, tectonic displacements will not be uniform, as points near the fault ends will have different displacements than their counterpoints located far from these ends. Finally, fault slip rates may vary with time and geomorphic transport may be subject to certain constraints, such as the lack of transportable material once bedrock is exposed. For this reason, flexible numerical solutions to these differential equations are necessary if we are to apply the principles of this simple transport process to a wide range of realistic geologic conditions.

3.3 Finite difference approximation

3.3.1 Taylor series and approximations of the first derivative

The finite difference method is based on the idea that derivatives and integrals of functions can be approximated by calculating discrete values of the equations when the differentiation or integration step is small. For example, in the difference quotient, which relates a function to its derivative, we approximate the limit of $dx \rightarrow 0$ by letting dx equal some arbitrarily small number. To do this, we first divide the solution space into discrete elements, separated by a uniform, but small distance, Δx . Each point (or node) in this space has a corresponding value of the function. In our example, we consider the location of the nodes to represent the distance along a topographic profile and their values to represent the elevation at a each location. If we need to compute the derivative (or slope) of the topography, we can use the Taylor Series approximation of a function at a point [Chapra and Canale, 1988; Ferziger, 1981]:

$$\begin{aligned} f(x_{i+1}) = & f(x_i) + f'(x_i)(x_{i+1} - x_i) + f'' \frac{x_i}{2!} (x_{i+1} - x_i)^2 \\ & + f''' \frac{x_i}{3!} (x_{i+1} - x_i)^3 + \dots + f^n \frac{x_i}{n!} (x_{i+1} - x_i)^n + R_n \end{aligned} \quad (3.7)$$

where R_n is a remainder term for terms $n+1$ to ∞ , and $f'(x_i)$ is the first derivative at x_i , etc. If we assume that the terms to the right of the first derivative that we are trying to compute (f') yield an answer that is small, we can truncate the remaining terms and solve for the value of the derivative:

$$\begin{aligned} f(x_{i+1}) &= f(x_i) + f'(x_i)(x_{i+1} - x_i) + R_1 \\ f'(x_i) &= \frac{f(x_{i+1}) - f(x_i)}{x_{i+1} - x_i} - \frac{R_1}{x_{i+1} - x_i} \end{aligned} \quad (3.8)$$

(1st order approximation – truncation error)

Then let $\Delta x = (x_{i+1} - x_i)$ [step size], and $\Delta f = f(x_{i+1}) - f(x_i)$ [first forward difference], so that the finite divided difference is

$$f'(x_i) = \frac{\Delta f}{\Delta x} - \frac{0}{\Delta x} \quad (3.9)$$

In the finite difference approach, we assume that the space step is uniform in the model space. Therefore, the denominator of 3.8 is equal to the uniform spacing (Δx). Importantly, in the above example, we have truncated the trailing terms in the Taylor series approximation, assuming that they are small relative to the value of the derivative we computed. This is conceptually the simplest way to compute a finite difference, but is definitely not the most accurate. Because only the first term of the Taylor Series was kept in our approximation, we term this method "first-order accurate." Generally, we desire methods that are more accurate than this for our approximations.

In the above derivation, we computed the derivative of the function by using the point located one step beyond the point at which the derivative was calculated. We could have just as easily elected to compute the derivative based on the previous point, located one step behind the point at which we wish to calculate the derivative. The preceding derivation is called the *forward finite difference* because it computes the derivative based on the point ahead of the point of the derivative, and the latter case is called the *backward finite difference*. It is computed in a similar way as the forward finite difference:

$$f(x_{i-1}) = f(x_i) - f'(x_i)\Delta x + f'' \frac{\Delta x^2}{2!} - \dots \quad (3.10)$$

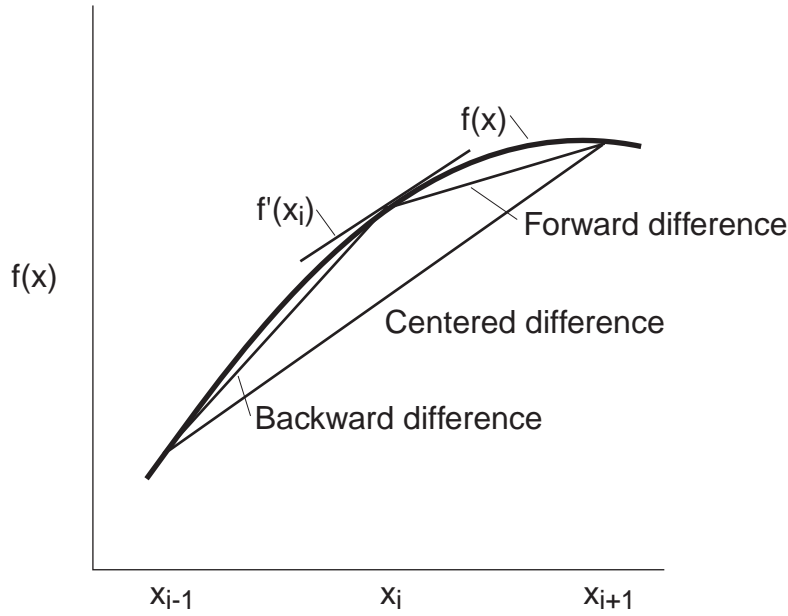


Figure 3.3: Graphical representation of various difference approximations of the slope (1st derivative; $f'(x_i)$) of a function and their relation to the true slope at that point. Note the increased accuracy of the centered difference.

By subtracting these two approximations, a far more accurate approximation (called the *centered finite difference*) of the derivative can be made:

$$\begin{aligned}
 f(x_{i+1}) &= f(x_{i-1}) + 2f'(x_i)\Delta x + f'''(x_i)\frac{\Delta x^3}{3!} + \dots \\
 f'(x_i) &= \frac{f(x_{i+1}) - f(x_{i-1}))}{2\Delta x} - \frac{f'''(x_i)}{6}\Delta x^2 \\
 f'(x_i) &= \frac{f(x_{i+1}) - f(x_{i-1}))}{2\Delta x} - 0\Delta x^2
 \end{aligned} \tag{3.11}$$

Equation 3.11 is the centered or central difference representation of the first derivative. Notice that it is second order accurate (we truncate after the second derivative). Figure 3.3 shows the geometry of these first derivative approximations.

3.3.2 Finite difference approximations of higher order derivatives

First, write a forward Taylor Series approximation of $f(x_{i+2})$ in terms of $f(x_i)$:

$$f(x_{i+2}) = f(x_i) + f'(x_i)(2\Delta x) + f''(x_i)\frac{2\Delta x^2}{2!} + \dots \tag{3.12}$$

Multiply 3.9 by 2 and subtract from 3.12 to yield

$$f(x_{i+2}) - 2f(x_{i+1}) = -f(x_i) + f''(x_i)\frac{2\Delta x^2}{2!} + \dots \tag{3.13}$$

Which is solved for

$$f''(x_i) = \frac{f(x_{i+2}) - 2f(x_{i+1}) + f(x_i)}{\Delta x^2} - \frac{0}{\Delta x} \quad (3.14)$$

That relationship is called the *second forward finite divided difference*. Similar manipulations can be employed to derive a backward version

$$f''(x_i) = \frac{f(x_i) - 2f(x_{i-1}) + f(x_{i-2}))}{\Delta x^2} - \frac{0}{\Delta x} \quad (3.15)$$

and a centered version

$$f''(x_i) = \frac{f(x_{i+1}) - 2f(x_i) + f(x_{i-1}))}{\Delta x^2} - \frac{0}{\Delta x^2} \quad (3.16)$$

As was the case with the 1st order approximations, the centered version is more accurate. Also notice that the centered version can alternatively be expressed as

$$f''(x_i) = \frac{\frac{f(x_{i+1}) - f(x_i)}{\Delta x} - \frac{f(x_i) - f(x_{i-1}))}{\Delta x}}{\Delta x} - \frac{0}{\Delta x^2} \quad (3.17)$$

Thus, just as the second derivative is the derivative of a derivative, the second divided difference approximation is a difference of two first divided differences.

3.4 Numerical solutions to the basic linear diffusion erosion problem

3.4.1 Derivation

Here we present an explicit finite difference method for solving equation 3.3 for arbitrary initial conditions (see Figure 3.4 for the temporal and spatial discretization grid and computational molecule).

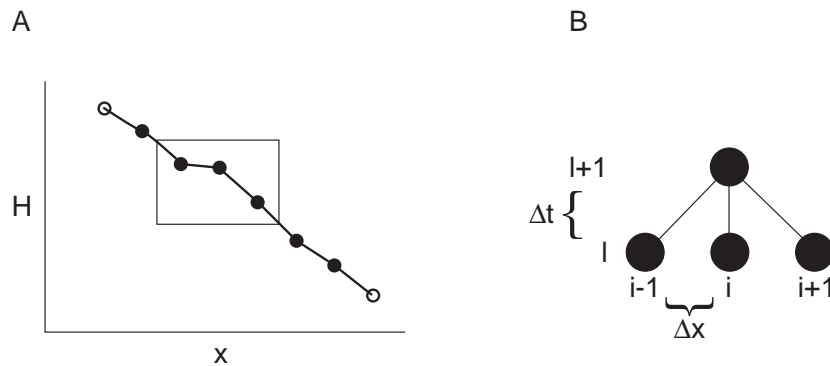


Figure 3.4: A) Discretized profile. Interior nodes are solid and their changes in elevation with time can be solved with the method described here, whereas the boundary node (open) elevations must always be specified. B) Computational molecule for three adjacent nodes within the profile (for example those boxed at left). Note how the elevation of the central point (i) in the future ($l + 1$) is a function of its elevation and that of its immediate neighbors at time l .

the time derivative (left hand side of 3.3) with a forward divided difference 3.9:

$$\frac{\partial H}{\partial t} \approx \frac{H_i^{l+1} - H_i^l}{\Delta t} \quad (3.18)$$

Note that we introduce the space index i (subscripted) and the time index l (superscripted). We assume no tectonic input and transport-limited conditions. Secondly, approximate the space derivative (right hand side of 3.3) by a centered divided difference 3.16:

$$\frac{\partial^2 H}{\partial x^2} \approx \kappa \frac{H_{i+1}^l - 2H_i^l + H_{i-1}^l}{\Delta x^2} \quad (3.19)$$

substitute 3.18 and 3.19 into 3.3 to yield the explicit finite difference approximation of the elevation at H_i^{l+1} as a function of its neighbor points at H_i^l . It provides an explicit means of computing values at each node for a future time, based on the present values.

$$\begin{aligned} \frac{H_i^{l+1} - H_i^l}{\Delta t} &= \kappa \frac{H_{i+1}^l - 2H_i^l + H_{i-1}^l}{\Delta x^2} \\ H_i^{l+1} &= H_i^l + \frac{\kappa \Delta t}{\Delta x^2} (H_{i+1}^l - 2H_i^l + H_{i-1}^l) \\ H_i^{l+1} &= H_i^l + \lambda (H_{i+1}^l - 2H_i^l + H_{i-1}^l) \end{aligned} \quad (3.20)$$

where $\lambda = \frac{\kappa \Delta t}{\Delta x^2}$. This equation is written for all interior nodes of the profile (Figure 3.4). This explicit method is convergent and stable for $\lambda \leq 1/2$, or $\Delta t \leq \frac{1}{2} \frac{\Delta x^2}{\kappa}$ (Ferziger, 1981).

3.4.2 Benchmarking the method—how accurate is it?

Whenever one uses an approximate method such as the FDM discussed here, it is appropriate to check its accuracy by comparing numerical results with those calculated analytically. Such a calculation has to be done within the stricter conditions of the analytical solution, but it lends confidence to the subsequent broader application of the numerical solutions.

As an illustration of the accuracy and behavior of the numerical method employed above, we "benchmark" it against the finite slope analytical solution (3.5) for a morphologic age of $\kappa t = 5 \text{ m}^2$ (Figure 3.5). In that figure, the upper panel shows that the two methods are graphically similar and that the error is small. The lower panel shows the difference between the analytical and numerical solutions and illustrates two important points: 1) The lower magnitude errors that are antisymmetric about the origin are due to the numerical inaccuracy. They correlate with the curvature of the model. 2) The larger magnitude errors at the end of the profile are the result of a difference between the boundary conditions of the numerical model (constant elevation) and the elevation change calculated analytically. The analytical model indicates that a morphologic age of 5 m^2 , elevation change (erosion and deposition) has reached the edges of the solution domain (-10 and 10 m). However, the numerical model fixes those boundary elevations and thus the two solutions diverge. To address this problem, the easiest thing to do is extend the numerical method boundaries far beyond the domain of interest (and increase the number of nodes if the same level of detail in the approximation is desired).

3.4.3 An example application of the 1-D explicit finite difference method solved using a spreadsheet (Microsoft Excel)

In Figures 3.6, 3.7, and 3.8, we illustrate how one might solve the diffusion erosion problem using a spreadsheet. Figure 3.6 is an example spreadsheet used to solve 3.3 by 3.20. The constants in solid boxes are input, and the spreadsheet determines the rest. Figure 3.7 shows the necessary Microsoft Excel formulae. In order to calculate to a given age, we must copy the D column to the right enough times to keep the calculation stable. For example, to determine the profile shown in Figure 3.8A, 100 time steps, or 100 columns were used. For the given parameters such a result is well within the stability criterion (unlike Figure 3.8B; a nice example of an unstable solution). These examples are limited in number of nodes for convenience. Simple

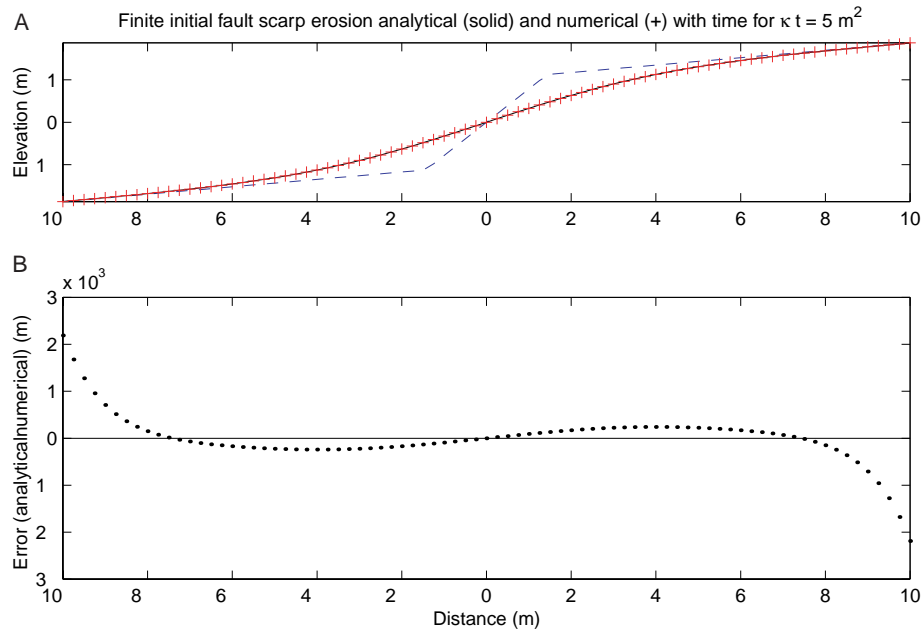


Figure 3.5: A) Comparison between analytical (solid line) and numerical (+) solutions to the diffusion erosion of the initial profile (dashed line) for $\kappa t = 5 \text{ m}^2$. B) Difference between analytical and numerical solutions. Errors are acceptably small and in the interior result from numerical inaccuracy and on the edges from the difference in boundary conditions (constant elevation for numerical method and elevation change for analytical method).

explorations with this tool can be very useful to build intuition about this geomorphic process, the importance of initial and boundary conditions, and the uniqueness of the morphologic age (κt) for form. More elaborate spreadsheets and simple exercises are available at

<http://www.public.asu.edu/~arrows/geomorph/diffuse/index.html>.

A *MATLAB* implementation of this method is available at

<http://activetectonics.la.asu.edu/diffuse/>

	A	B	C	D	E	F	G	H
1	Simple spreadsheet to do diffusion erosion							
2								
3	Constants:		units					
4	dx=	4	m					
5	dt=	0.05	kyr					
6	k=	1	m^2/kyr					
7	lambda=	0.003125						
8	age=	5	kyr					
9								
10			I (time)->					
11			0	0.05	0.1	0.15	0.2	0.25
12	x	I (distance)	1	2	3	4	5	6
13	-10	0	-1	-1	-1	-1	-1	-1
14	-6	1	-1	-1	-0.99998	-0.99994	-0.99988	-0.99981
15	-2	2	-1	-0.99375	-0.98756	-0.98143	-0.97535	-0.96933
16	2	3	1	0.99375	0.987559	0.981425	0.975349	0.96933
17	6	4	1	1	0.99998	0.999942	0.999884	0.999808
18	10	5	1	1	1	1	1	1

Figure 3.6: Example Microsoft Excel Spreadsheet for explicit finite difference. The values inside the bold boxes can be changed and the result plotted in a chart. Figure 3.7 shows the equivalent spreadsheet with the formulae displayed.

	A	B	C	D
1	Simple spreadsheet			
2				
3	Constants:		units	
4	dx=	4	m	
5	dt=	0.05	kyr	
6	k=	1	m^2/kyr	
7	lambda=	= (k*dt)/dx^2		
8	age=	=CY11	kyr	
9				
10			I (time)->	
11			=C12*dt-dt	=D12*dt-dt
12	x	I (distance)	1	2
13	=-10+B13*dx	0	-1	=C13
14	=-10+B14*dx	1	-1	=C14+lambda*(C15-2*C14+C13)
15	=-10+B15*dx	2	-1	=C15+lambda*(C16-2*C15+C14)
16	=-10+B16*dx	3	1	=C16+lambda*(C17-2*C16+C15)
17	=-10+B17*dx	4	1	=C17+lambda*(C18-2*C17+C16)
18	=-10+B18*dx	5	1	=C18
19				
20				

Figure 3.7: Example Microsoft Excel Spreadsheet for explicit finite difference with formulae shown.

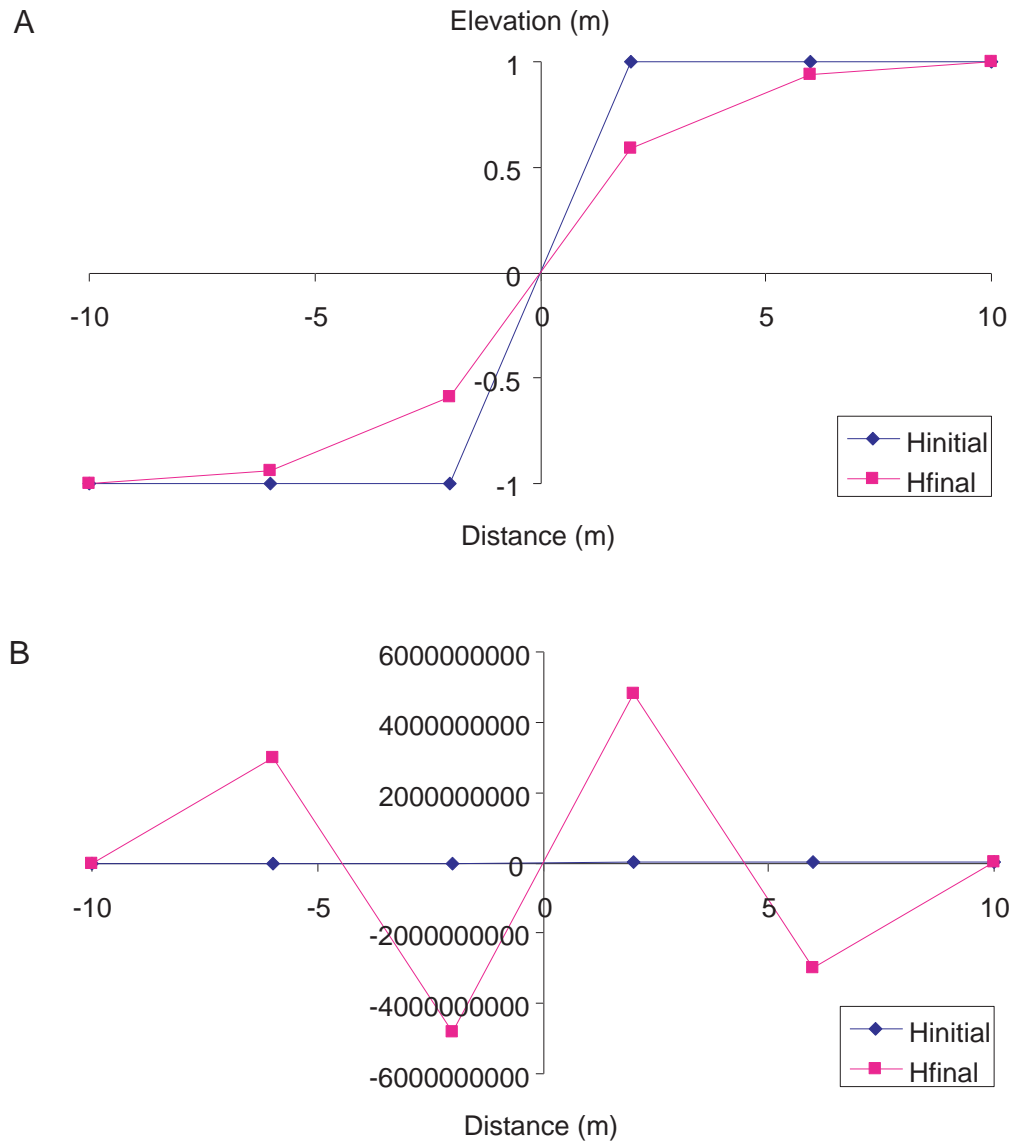


Figure 3.8: Microsoft Excel plots showing the initial and final profiles determined using the sample spreadsheet (Figures 3.6 and 3.7). A) Diffusion erosion solution for degraded step; 1-D explicit finite difference technique, $t = 5$ kyr, $\kappa = 1 \text{ m}^2/\text{kyr}$. B) Unstable diffusion erosion solution for degraded step; 1-D explicit finite difference technique, $t = 1000$ kyr, $\kappa = 1 \text{ m}^2/\text{kyr}$ (with a large $\lambda = 0.625$; exceeding the stability criterion).

Chapter 4

How to use the software

4.1 Introduction

In this chapter, we describe how a practitioner may use the Penck1D model to simulate fault scarp development. We created a Graphical User Interface (GUI) to the finite difference code that aids in the creation, display, and analysis of the fault scarp models. In particular, we have created a variety of functions that allow location (X), topography (Z), and bedrock elevation (B) to be imported into the software and interpolated to form the initial conditions of the model. Easy entry of model parameters is facilitated by the interface. Also, we provide functions to create and manipulate a number of simple initial conditions. Finally, we provide routines that allow the initial conditions, fault geometry and displacements, and model results to be easily plotted.

In the sections that follow, we outline the operation of the GUI and how the user can change the model parameters for the simulation. Then, we introduce the reader to the different menu functions that may be used to import or export data, manipulate imported data, set initial conditions, run models, and plot the results. Finally, we give a series of examples that will help illustrate the practical operation of the program.

4.2 Using the program

4.2.1 A note about units

Penck1D does not use a specific set of units. Therefore, the choice of the units is up to the user. However, it is important to use consistent units for each of the model parameters. The default settings correspond to an example set of values in the following units: [L]ength units, meters; and [t]ime units, years. When using different units, make sure to convert all values into the same units before running a model.

4.2.2 Starting the program

Penck1D uses built-in routines of the MATLAB software, available from the MathWorks. Make sure to properly install this software before trying to use the Penck1D program.

In order to use Penck1D, launch Matlab, and then type “penckgui” at the prompt:

```
>> penckgui
```

This will start the Penck1D interface.

4.2.3 General model building procedure

Building a scarp model consists of the following steps:

1. **Set model parameters.** Values specifying the fault geometry and rates, geomorphic transport rates, and bedrock production rates must be specified. Do this by modifying the default example values that are specified when the program is started.
2. **Import and grid X, (B), H data.** Data may be read from a text input file that specifies the initial topography (H) and bedrock elevation (B) for the model. Once the data are imported, they may be interpolated to form a profile that is appropriate for the model.
3. **Set initial conditions.** Gridded input data may be applied to the initial conditions of the model (topography and bedrock elevation), or simple initial geometries may be specified. Examples of these simple initial geometries are flat and sloping surfaces.
4. **Run model.** Either transport- or production-limited models may be run. If production-limited conditions are not expected to be important, run a transport-limited model for computational efficiency.
5. **Plot results.** Initial conditions, fault geometry, fault displacements, and time snapshots of fault development may be plotted.
6. **Save or export data.** Model results may be saved for future viewing or exported as X, (B), H text files that can be read by a variety of common plotting packages, such as Microsoft Excel.

4.2.4 Setting model parameters

The first step in building a model is specifying the rates of movement along and geometry of the fault. In addition, geomorphic transport rates, regolith production rates, and boundary conditions at the left and right sides of the profile must be specified. All of these model parameters may be set in the Penck1D main window.

In Figure 4.1, we have labeled each of the areas that correspond to the values. The labels, parameter, and dimensions of each of the model parameters are outlined in Table 4.1. To change each of the model values, use the cursor to select the value, and change it as appropriate. Values will not be modified if they contain invalid information (e.g., value out of parameter range or letters in a numeric entry).

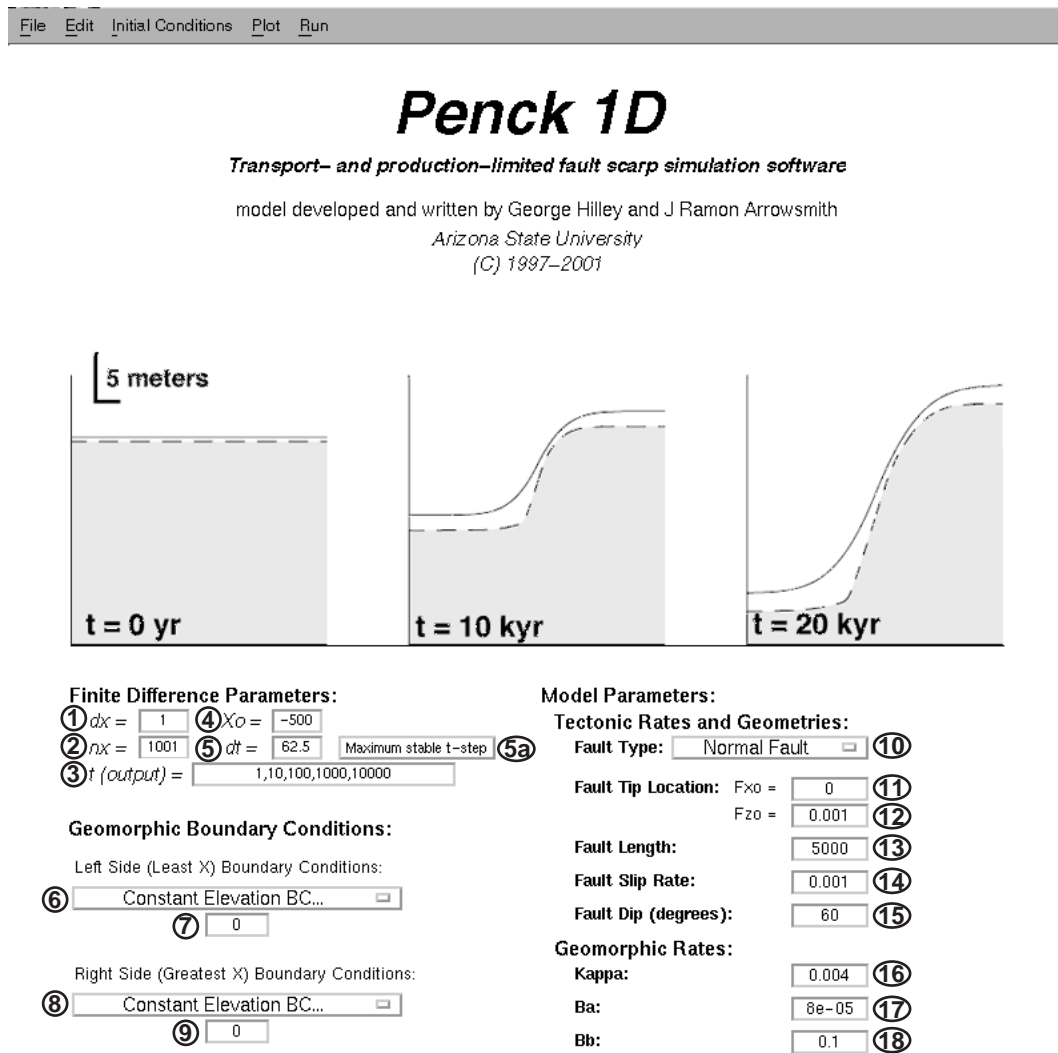


Figure 4.1: Main screen (with labeled parameters) for Penck1D software. See Table 4.1 for meaning, units, and common values of model parameters.

Table 4.1: Model Parameters and typical values. Numbers refer to Figure 4.1

#	Symbol	Parameter	Dimensions	Default Value
1	dx	Model Spacing	[L]	1 m
2	nx	Number of Points in Model	N/A	1001
3	$t(output)$	Time at which output is recorded	[t]	1, 10, 100, 1000, 10000 yr
4	X_o	Left hand location of profile	[L]	-500 m
5	dt	Time step	[t]	62.5 yr
5a	N/A	Maximum stable dt button	N/A	N/A
6	LBCTYPE	Left side boundary condition type	N/A	Constant Elevation
7	LBC	Left side boundary condition value	*	0
8	RBCTYPE	Right side boundary condition type	N/A	Constant Elevation
9	RBC	Right side boundary condition value	*	0
10	Fault Type	Sense of slip on fault	N/A	Normal Fault
11	Fx_o	X-coordinate of upper fault tip	[L]	0 m
12	Fz_o	Z-coordinate of upper fault tip	[L]	0 m
13	L	Fault Length	[L]	5000 m
14	b	Fault Slip Rate	[L/t]	0.001 m/yr
15	β	Fault Dip	[°]	60°
16	κ	Hillslope diffusivity	[L ² /t]	0.004 m ² /yr
17	B_a	Surface Regolith Production Rate	[L/t]	8×10^{-5} m/yr
18	B_b	Regolith Production Depth Scaling Factor	[1/L]	0.1 m ⁻¹

* denotes parameters whose dimension varies according to boundary condition type. Boundary condition types “Constant Elevation” and “Constant Flux” produce dimensions of [L] and [L²/t], respectively.

The t (*output*) entry (3) specifies the times at which model output is desired. This may be entered as a comma-delimited list of numbers. For example, if output is desired at times of 10, 30, 40, and 1000, highlight the values in the t (*output*) box and type 10, 30, 40, 1000.

The *Maximum stable t-step* button (5a) resets the value of the time step, dt (5) to its maximum allowable value. In the case that a smaller dx is entered, the value of dt is adjusted to maintain stability. If a larger value of dx is entered, the value of dt is not adjusted because it is allowable to have time steps smaller than the stability criterion but not larger. Pressing the *Maximum stable t-step* button ensures that the time step is appropriate for the value of κ and dt being used.

Note: The criterion for stability in a one dimensional diffusive model is $\Delta t = 0.5 \times dx^2/\kappa$. However, we allow a maximum time step of $\Delta t = 0.1 \times dx^2/\kappa$ to maintain some degree of accuracy in the solution.

The types of boundary conditions prescribed at the model edges may be changed using the pull-down menus shown in Figure 4.2. The left and right boundary conditions may be changed using the (6) and (8) pulldown menus, respectively.

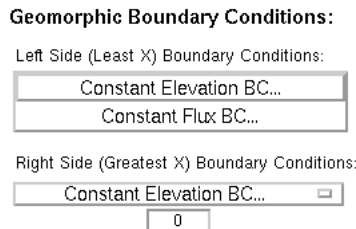


Figure 4.2: Popup used to change boundary conditions. Click and hold on (6) or (8), and drag the menu to select the appropriate boundary condition type.

4.2.5 Menu functions

File menu

Basic functions for reading and writing files are found in the **File** Menu (Figure 4.3). The **New** function (FM1) clears all variables to their default values, erases any imported data, and deletes the current model results. When this option is selected, a dialogue box (Figure 4.4) is displayed to make sure that all model variables should be cleared. **Open...** (FM2) is used to load a previously saved Penck1D session that was saved using the **Save As...** function (FM3). The **Save As...** function saves any current model results and all model parameters, imported data, and gridded data in a Matlab **.mat** file that can be read into Matlab for later use. All of these functions initiate a dialogue that requires the name of the file to be opened or saved to be selected or typed.

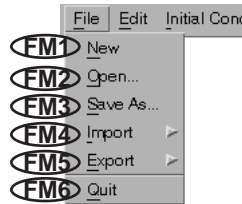


Figure 4.3: File menu for Penck1D.

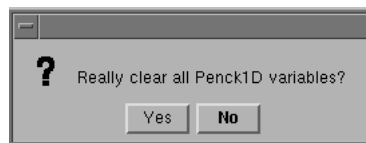


Figure 4.4: Dialogue box to confirm all variables should be cleared.

Data can be imported and exported as text files using the **Import** (FM4) and **Export** (FM5) submenus. Exported files can be read into spreadsheet or plotting programs such as Microsoft Excel and imported files may be used to import complex initial profile geometries into Penck1D. The **Import** and **Export** menus are shown in Figures 4.5 and 4.6, respectively.

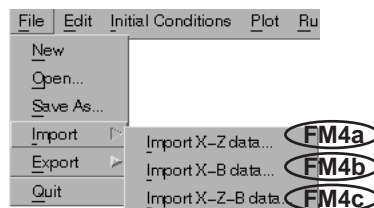


Figure 4.5: Import submenu for Penck1D.

Three different types of files may be imported and used as initial conditions in a Penck1D model. First, a file containing location and elevation points (X-H data) may be imported using **Import X-Z data...** (FM4a). Each point consists of an X and H value separated by spaces or tabs. Each line of the file should contain one corresponding X-H pair. For example, if the three measured coordinates of $(-5, 1)$, $(0, 0)$, and $(5, 3)$ are to be imported, the file should look like:

```
-5      1
0       0
```

5

3

In addition, if a measured or complicated initial bedrock profile is to be imported, use **Import X-B data...** (FM4b). The input text file should have identical syntax as the previous example, except that the elevation values should be replaced by the bedrock elevation values.

If values of topographic and bedrock elevation are recorded for identical points, use the **Import X-Z-B data...** (FM4c) to use these data for the initial profile and bedrock conditions. The file syntax is similar to the above two examples, except that each point contains three values and so must have the location, profile elevation, and bedrock elevation values in each line. For example, if the (X, Z, B) values that you wish to import are $(-5, 4, 2)$, $(0, 5, 1)$, and $(5, 2, -5)$ the input file should have the following syntax:

-5	4	2
0	5	1
5	2	-5

In addition, model results and parameters can be saved to a text file that can then be used in other plotting and analysis programs. Figure 4.6 shows the export options that are available in Penck1D. Importantly, exported files cannot be directly read back into Penck1D using the **Open...** (FM2) or **Import** submenu (FM4) functions. In order to save all parameters and model results in a format recoverable by Penck1D, use the **Save As...** command (FM3).

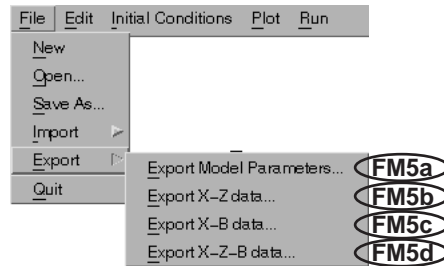


Figure 4.6: Export submenu for Penck1D.

Several different types of data can be exported from Penck1D. First, the model parameters can be exported into a file for later reference using the **Export Model Parameters...** function (FM5a). Second, the location and elevation data from the model results may be exported using the **Export X-Z data...** (FM5b) command. Third, if the bedrock elevation is desired, use the **Export X-B data...** (FM5c) command. Finally, if all of the model results should be exported into a text file, use the **Export X-Z-B data...** (FM5d) command. Importantly, exporting any model elevation results (FM5b–d) will also export the model parameters at the beginning of the file.

If the type of output chosen is elevation data (FM5b–d), the times at which the data should be output must be selected. For example, if model results were collected at $t_{\text{output}} = 1, 10, 1000, 10000, 100000$, and you wish to write out only 10000 and 100000, you must select these times in the following manner. After selecting the type of data you wish to export, you will be confronted with the dialogue box shown in Figure 4.7. To select the proper times, click on 10000 and 100000 (solid arrows) to select the desired model times. Next, click on 0 (open white arrow) to unselect 0 as an output model time. Next, click **Continue** and you will be presented with a dialogue box that allows specification of the output file name.

Finally, to quit Penck1D, select the **Quit** option from the **File** menu (FM6). This presents the dialogue box shown in Figure 4.8, confirming that you wish to quit Penck1D.

Edit menu

The **Edit** menu (Figure 4.9) allows manipulation of imported data. When (x, H) , (x, B) , or (x, H, B) data is imported into the program, it must be interpolated to contain surface and/or bedrock elevation values at

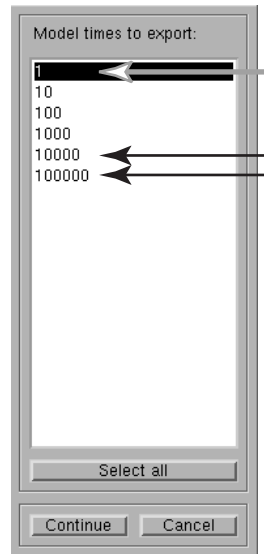


Figure 4.7: Dialogue box to select times to export model topography to text file.

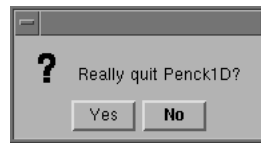


Figure 4.8: Dialogue box confirming exit from Penck1D.

each model location defined by X_o , dx , and nx . After interpolation of the imported data has been performed, the original imported data is kept in the event that the X_o , dx , or nx values are changed. If these values are changed, the imported data must be reinterpolated to accommodate the new model profile parameters. Functions in the **Edit** menu provide tools with which to modify the imported data and interpolate (grid) these data into a surface or bedrock profile that can be applied to the initial conditions using the **Initial Conditions** menu.

The first function in the **Edit** menu allows exchange of the imported bedrock elevations (**Bedrock**) and surface elevations (**Profile**) data. For example, if data imported as **Profile** data should be used as the bedrock elevations, switch the two using the **Switch Import Data (bedrock->profile, profile->bedrock)** (EM1).

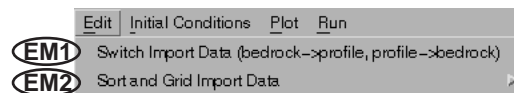


Figure 4.9: Edit menu for Penck1D.

Once data has been imported and properly stored in Penck1D, it must be interpolated into a profile for which there are elevation values at regularly spaced points. This spacing is defined by the dz parameter. To perform this interpolation, use the **Sort and Grid Import Data** submenu (EM2). Here, select **Profile Import Data** (EM2a) or **Bedrock Import Data** (EM2b) if you would like to grid the surface and bedrock elevation data, respectively, imported using the **Import** submenu (FM4) of the **File** menu.

Note: Each time the model parameters that define the spacing, location, and length of the profile are changed, the imported data must be regridded. Failure to do so will result in an error.

Note: It is possible to use imported profile points that do not span the full model space defined by the

X_o , dx , and nx values. This results in a lack of data with which to interpolate the profile and/or bedrock values at one or both of the two ends of the model. If this situation arises, Penck1D automatically assumes that the extreme locations of the model have the elevation of the nearest imported point.



Figure 4.10: Sort and Grid submenu for Penck1D.

Initial conditions menu

The **Initial Conditions** menu is used to set the initial profile and bedrock geometry of the model. This geometry can be a simple, theoretical geometry, or one that is measured or inferred in the field and imported into the model using the **Import** (FM4) and **Sort and Grid Import Data** (EM2) submenus discussed previously.

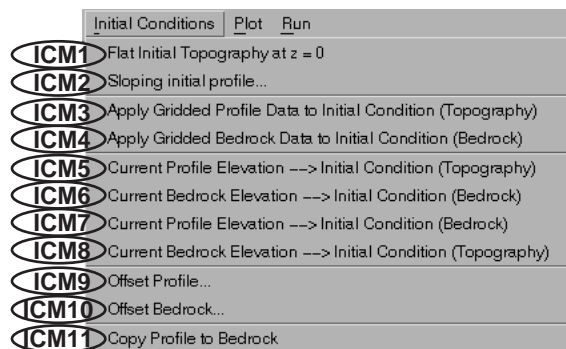


Figure 4.11: Initial conditions menu for Penck1D.

Simple initial topographies may be specified using the first two functions in the **Initial Conditions** menu. The **Flat Initial Topography at $z=0$** (ICM1) sets the profile (surface) surface elevation values to zero at the spacing, location, and length specified by X_o , nx , and dx . Importantly, the bedrock elevations are not affected by this function. In addition, sloping initial surfaces may be specified using the **Sloping initial profile...** (ICM2) function. A dialogue box then appears (Figure 4.12) that requests the angle of the sloping surface. In our model, negative and positive angles specify surfaces that slope to the right and left, respectively. Again, the bedrock elevation is unaffected by this function.

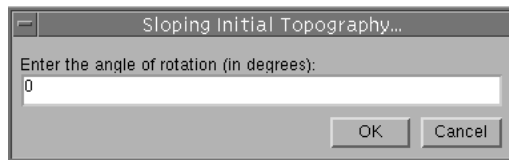


Figure 4.12: Dialogue box requesting input for a sloping surface initial condition.

To apply imported and previously gridded data to the profile (surface) or bedrock elevation initial conditions, use the **Apply Gridded Profile Data to Initial Condition (Topography)** and **Apply Gridded Bedrock Data to Initial Conditions (Bedrock)** functions. These copy the profile and bedrock data gridded by the **Sort and Grid Import Data > Profile Import Data** (EM2a) and **Sort and Grid Import Data > Bedrock Import Data** (EM2b), respectively, to the specified initial condition.

In addition, profiles produced as model results may be applied as initial conditions. The next four functions (ICM5–8) apply the last calculated and recorded model profile and bedrock values to the initial conditions of a new model. (ICM5) applies the final profile model results to the topography initial condition, (ICM6) applies the final bedrock model profile to the bedrock initial condition, (ICM7) applies the final elevation values to the bedrock initial condition, and (ICM8) applies the final bedrock values to the profile initial condition.

The surface or bedrock profiles may be offset by a uniform elevation using the **Offset Profile...** (ICM9) and **Offset Bedrock...** (ICM10) functions, respectively. These functions trigger a dialogue box that requests the input of a uniform offset for the profile (ICM9; Figure 4.13) or bedrock (ICM10). For example, if one wished to text a uniform decrease in regolith thickness on a model whose initial conditions were imported from a text file, the bedrock elevation could be increased the amount that corresponded to the decrease in regolith thickness. Finally, the initial conditions specified for the surface elevations may be copied to the bedrock elevations using the **Copy Profile to Bedrock** (ICM11) command. This command is especially useful for constructing simple initial conditions in which the bedrock elevations parallel the surface elevations. By copying the profile elevations to the bedrock elevations using (ICM11) and then offsetting the bedrock by a uniform thickness equal to the initial regolith thickness (ICM10), a situation in which a uniform-regolith landscape can be constructed.



Figure 4.13: Dialogue box requesting a uniform offset for surface elevation (Profile) data.

Plot menu

The **Plot** menu is used to display different aspects of the model including initial conditions, fault geometry, fault displacements, and the coupled geomorphic and tectonic model results. Figure 4.14 shows the different items in the menu. In addition, any plots can be saved, printed, or exported to different file formats (such as Encapsulated Postscript or Adobe Illustrator formats) for direct inclusions in reports or research documents.

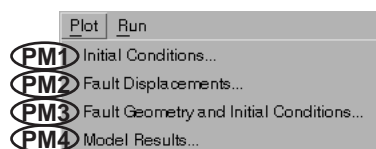


Figure 4.14: Plot menu for Penck1D.

The model initial conditions can be displayed by selecting the **Initial Conditions ...** option (PM1) in the **Plot** menu. If the initial conditions are properly assigned, a window similar to that shown in Figure 4.15 opens, displaying the initial conditions. In this plot, the surface, bedrock/regolith interface, and bedrock are shown with a solid line, dashed line, and gray shading, respectively. This window is a good place to make sure that the initial conditions you desire are in fact those used in the current model. To zoom in on a particular part of the figure, use the magnifying glass tool on the toolbar or select **Zoom** from the **Tools** menu of this window. Finally, the window can be printed, saved to a Matlab figure file, or exported to variety of file formats (including EPS, Adobe Illustrator, TIFF, and JPEG) using the functions in the **File** menu of this window. See the Matlab command reference for more details on printing, saving, or exporting figures.

To display the fault displacements that result from fault slip in the model, use the **Fault Displacements ...** option (PM2) in the **Plot** menu. This function calculates the displacements due to movement along the fault during one increment of time (slip rate $\times t$). An example of this display is shown in Figure 4.16.

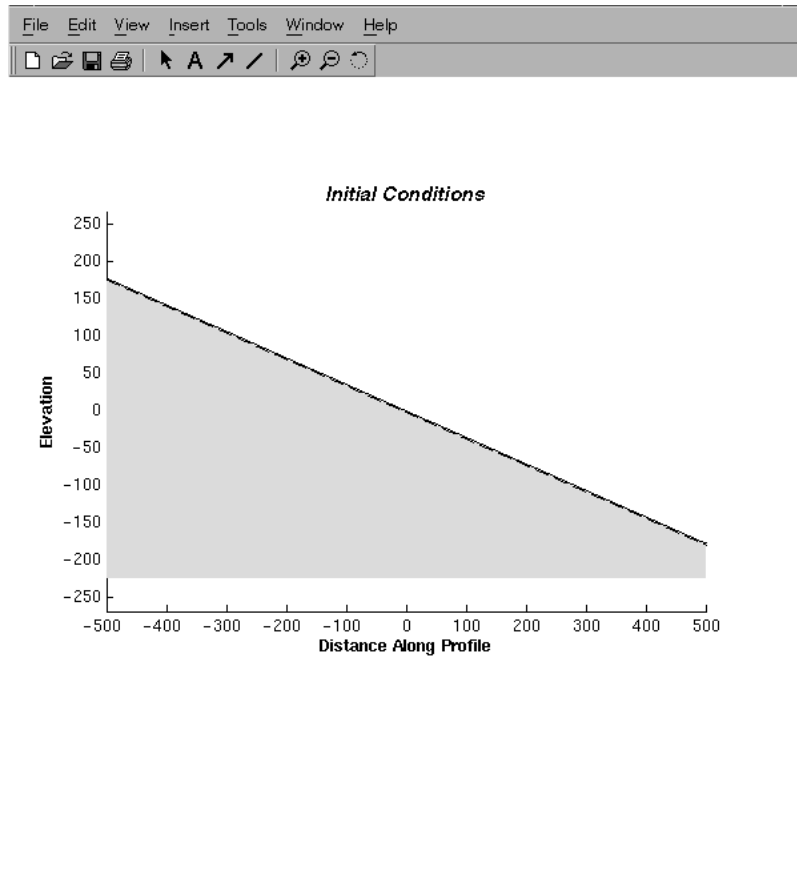


Figure 4.15: Window displaying initial conditions and fault geometry for the current model.

There are four major parts to this figure: 1) the upper-left frame shows the schematic fault geometry and location of the profile plotted relative to the fault length. The second and third graphs (full width) show the magnitude of the horizontal and vertical surface displacements, respectively due to fault slip. Finally, the lowermost graph shows a vector diagram of the two displacement components along the surface profile. The length of each vector is scaled to the magnitude of the displacement, with the scale shown in the upper right hand portion of the graph.

Both the fault geometry and initial conditions can be displayed using the **Fault Geometry and Initial Conditions ...** selection (PM3). An example of the plot created using this command is shown in Figure 4.17. As with all of the plotting functions, the graphs may be rescaled, saved, printed, and/or exported using the various functions in the **Tools** and **File** menus of the plot's window.

Finally, once a model has been run, the results may be viewed with the **Model Results ...** function (PM4). Selecting this function displays the figure shown in Figure 4.18. As with all of the other plots, zoom functions may be used to view details of the profiles. In addition, the **No Vertical Exaggeration** button removes all exaggeration in the figure, allowing the viewer to see the true geometry of the degraded scarp and bedrock elevation.

To view different profiles recorded at times $t(output)$, use the $t =$ pulldown menu shown in Figure 4.19. For instance, to view the profile at the final time ($t = 10000$), click on the pulldown menu, drag to 10000, and select this item. The model results at this time will then be displayed in the figure.

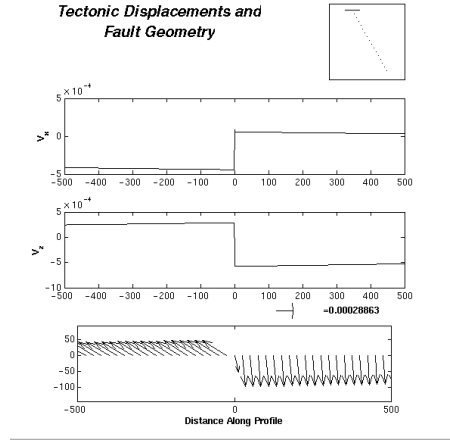


Figure 4.16: Plot of displacements and fault geometry for current model settings. Upper right figure shows fault geometry, upper graph shows horizontal displacements, middle graph shows vertical displacements, and bottom graph shows vector plot of displacements.

Run menu

The **Run** menu is used to run the scarp simulation for the model parameters and initial conditions specified (Figure 4.20). One can run a transport limited or production limited model by selecting the **Run Transport Limited Model (RM1)** and **Run Production Limited Model (RM2)**, respectively. Usually, if only transport-limited conditions exist, using (RM1) increases the computational performance slightly.

Once a model is started, a dialogue box will appear that shows the progress of the model (Figure 4.21). Once the model has successfully finished, a dialogue box will appear to alert the user of this (Figure 4.22).

4.3 Examples of fault scarp simulation

The following examples are intended to familiarize the reader with some of the steps required to run a Penck1D model, view the results, and export the data. The examples are meant to be used as exercised to increase the proficiency of the use of the program. The examples only contain production limited conditions; however, transport limited models may be developed and run in a similar manner as the examples.

4.3.1 Example 1: Flat initial topography offset by reverse faulting

In this example, we run and display the morphologic development of a scarp with moderate transport rates ($0.004 \text{ m}^2/\text{yr}$), regolith production rates typical for the Bay Area of California (80 m/Myr), with a depth scaling factor of (0.01 cm^{-1}), a 10 km long (downdip length) 45° dipping normal fault that slips at 10 mm/yr , with a flat initial surface topography with a uniform regolith mantle of 40 cm . In the example, we model the scarp profile from -500 m to $+500 \text{ m}$. For simplicity, we do not allow regolith transport in or out of the left or right side boundaries. This results in flux boundary conditions equal to zero at the left and right boundaries.

Follow the following steps to build the model:

1. Set model parameters:
 - Set $X_o = -500$ to set the left-most model location to -500 m .
 - Set $dx = 1$ to create a model with node spacing of 1 m .
 - Set $nx = 1001$ so that the profile ends at 500 m .

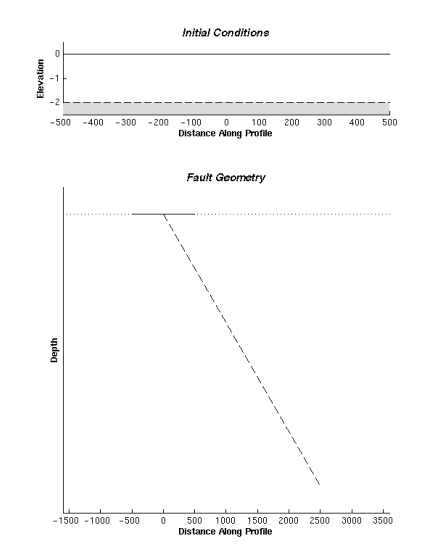


Figure 4.17: Plot of the fault geometry and initial conditions of the current model. This plot is useful for making sure that the desired initial conditions and fault geometry are selected.

- Click **Maximum stable t-step** button to set stable time step.
 - Set boundary condition types (both left and right) to constant flux using the pulldown menus.
 - Set fault dip to 45.
 - Set fault type to **Normal Fault** using the **Fault Type** pulldown menu.
 - Set fault length to 10000 (10 km = 10000 m; use consistent units).
 - Set fault slip rate to 0.01 (m/yr).
 - Set κ (κ) to 0.004 (m²/yr).
 - Set $B_a = 0.00008$ (m/yr).
 - Set $B_b = 1$ (m⁻¹).
2. Set Initial Conditions:
 - Create an initially flat topography, by using the **Flat Initial Topography at z=0** from the **Initial Conditions** menu.
 - Copy this flat surface topography to the initial bedrock topography using the **Copy Profile to Bedrock** function from the **Initial Conditions** menu.
 - Offset the bedrock profile -0.4 m using the **Offset Bedrock...** from the **Initial Conditions** menu.
 3. Plot pre-model data (printing, saving, and/or exporting figures as desired):
 - Plot initial conditions using the **Initial Conditions ...** function from the **Plot** menu.
 - Plot displacements using the **Displacements ...** item from the **Plot** menu.
 - Plot initial conditions and fault geometry using the **Fault Geometry and Initial Conditions ...** from the **Plot** menu.
 4. Run model: use **Run Production Limited Model** item from the **Run** menu.
 5. Plot Results:
 - View model results for different simulation times using the **Model Results ...** option from the **Plot** menu.

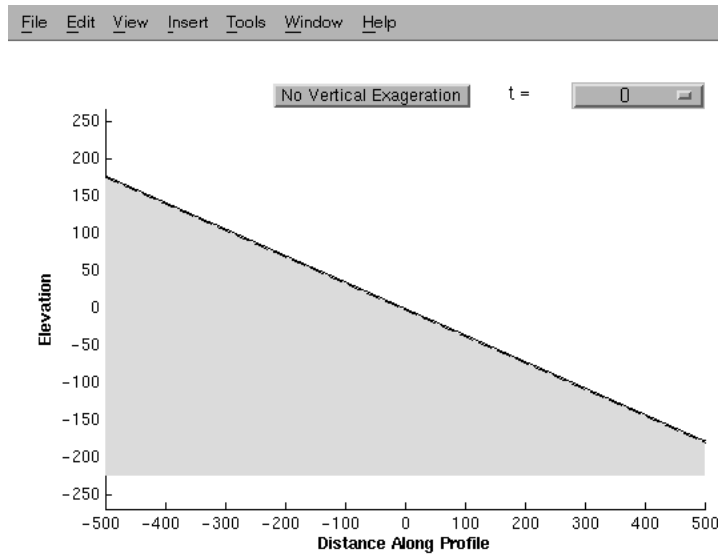


Figure 4.18: Model results plot. In this figure, the initial conditions are displayed ($t = 0$).

- Save figures as EPS files for later printing and analysis using **Export ...** option from the **File** menu of the plot window.

6. Save Model:

- Save model using the **Save As ...** option from the **File** menu
- Export the model results as an X, Z, B file for the last time step, using the **Export ...** submenu of the **File** menu.

4.3.2 Example 2: Sloping initial topography offset by normal faulting

This next example will use identical parameters as Example 1; however, the initial surface and bedrock elevations will slope 10° to the right.

1. Set model parameters:

- Set $X_o = -500$ to set the left-most model location to -500 m.
- Set $dx = 1$ to create a model with node spacing of 1 m.
- Set $nx = 1001$ so that the profile ends at 500 m.
- Click **Maximum stable t-step** button to set stable time step.
- Set boundary condition types (both left and right) to constant flux using the pulldown menus.
- Set fault dip to 45.
- Set fault type to **Normal Fault** using the **Fault Type** pulldown menu.
- Set fault length to 10000 (10 km = 10000 m; use consistent units).
- Set fault slip rate to 0.01 (m/yr).
- Set κ (κ) to 0.004 (m^2/yr).
- Set $B_a = 0.00008$ (m/yr).
- Set $B_b = 1$ (m^{-1}).

2. Set Initial Conditions:

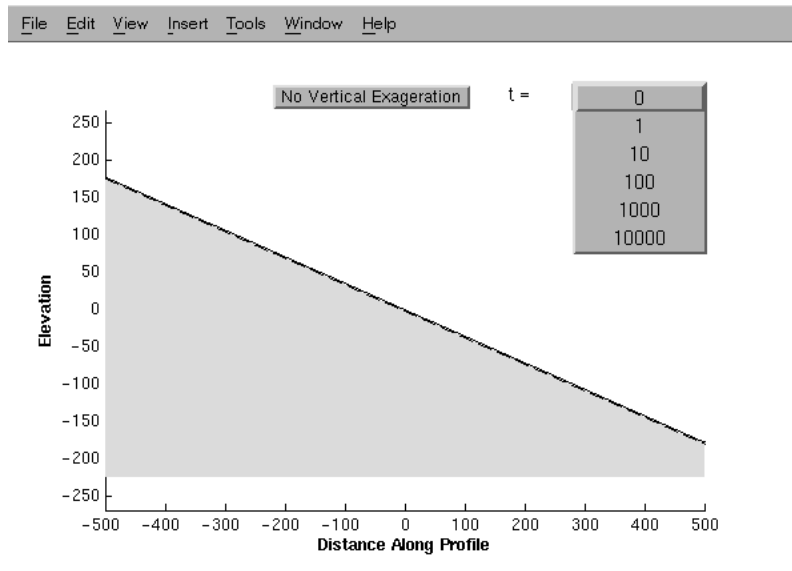


Figure 4.19: Model results plot, showing time pull-down menu.



Figure 4.20: Run menu in Penck1D.

- Create a sloping surface topography, by using the **Sloping initial surface ...** from the **Initial Conditions** menu. Fill in -10 in the next dialogue box.
 - Copy this sloping surface topography to the initial bedrock topography using the **Copy Profile to Bedrock** function from the **Initial Conditions** menu.
 - Offset the bedrock profile -0.4 m using the **Offset Bedrock...** from the **Initial Conditions** menu.
3. Plot pre-model data (printing, saving, and/or exporting figures as desired):
 - Plot initial conditions using the **Initial Conditions ...** function from the **Plot** menu.
 - Plot displacements using the **Displacements ...** item from the **Plot** menu.
 - Plot initial conditions and fault geometry using the **Fault Geometry and Initial Conditions ...** from the **Plot** menu.
 4. Run model: use **Run Production Limited Model** item from the **Run** menu.
 5. Plot Results:
 - View model results for different simulation times using the **Model Results ...** option from the **Plot** menu.
 - Save figures as EPS files for later printing and analysis using **Export ...** option from the **File** menu of the plot window.
 6. Save Model:
 - Save model using the **Save As ...** option from the **File** menu
 - Export the model results as an X, Z, B file for the last time step, using the **Export ...** submenu of the **File** menu.

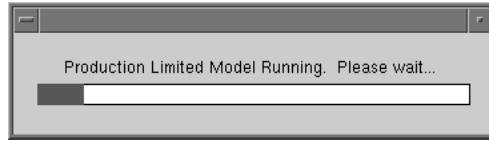


Figure 4.21: Dialogue box showing model progress.

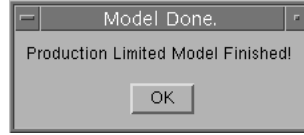


Figure 4.22: Run menu in Penck1D.

4.3.3 Example 3: Measured initial topography (imported data) offset by normal faulting

This example will use identical parameters to Example 1; however, we will use imported data to create the initial conditions.

1. Set model parameters:

- Set $X_o = -500$ to set the left-most model location to -500 m.
- Set $dx = 1$ to create a model with node spacing of 1 m.
- Set $nx = 1001$ so that the profile ends at 500 m.
- Click **Maximum stable t-step** button to set stable time step.
- Set boundary condition types (both left and right) to constant flux using the pulldown menus.
- Set fault dip to 45.
- Set fault type to **Normal Fault** using the **Fault Type** pulldown menu.
- Set fault length to 10000 (10 km = 10000 m; use consistent units).
- Set fault slip rate to 0.01 (m/yr).
- Set κ (κ) to 0.004 (m²/yr).
- Set $B_a = 0.00008$ (m/yr).
- Set $B_b = 1$ (m⁻¹).

2. Set Initial Conditions:

- Import the X, Z data from the file “sampleprof.xz” using the **Import ...** submenu of the **File** menu.
- Import the X, B data from the file “samplebr.xb” using the **Import ...** submenu of the **File** menu.
- Grid imported X, Z data using the **Sort and Grid import data** submenu from the **Edit** menu.
- Grid imported X, B data using the **Sort and Grid import data** submenu from the **Edit** menu.
- Apply the gridded data (both Profile and Bedrock) to the appropriate initial condition using the **Initial Conditions** menu.

3. Plot pre-model data (printing, saving, and/or exporting figures as desired):

- Plot initial conditions using the **Initial Conditions ...** function from the **Plot** menu.

- Plot displacements using the **Displacements ...** item from the **Plot** menu.
 - Plot initial conditions and fault geometry using the **Fault Geometry and Initial Conditions ...** from the **Plot** menu.
4. Run model: use **Run Production Limited Model** item from the **Run** menu.
 5. Plot Results:
 - View model results for different simulation times using the **Model Results ...** option from the **Plot** menu.
 - Save figures as EPS files for later printing and analysis using **Export ...** option from the **File** menu of the plot window.
 6. Save Model:
 - Save model using the **Save As ...** option from the **File** menu
 - Export the model results as an X, Z, B file for the last time step, using the **Export ...** submenu of the **File** menu.

Chapter 5

Final Thoughts: Validity of scarp modeling approach

The Penck1D model requires that the topography is continuous along the profile length and all deformation results from elastic deformation of the crust. In nature, a first-order feature of faults is that they offset material, thus creating a discontinuity in a structural datum. For instance, sufficiently large reverse fault offsets in scarp models may cause adjacent nodes in the finite-difference model to overlap in space. While this is a physically reasonable condition, the solution method requires the topography to be continuous and the node spacing to be uniform. In order to circumvent this problem, the model reinterpolates the elevation profile at every time step and relocates the fault tip location to remain at its prescribed location. In reality, a thrust plate may ride over the surface of the preexisting topography for large distances, deforming the hangingwall at the surface into a fault bend fold [Lave and Avouac, 2000; Wesnousky *et al.*, 1999; Arrowsmith *et al.*, 1999b]. These scenarios are not modeled for the following reasons: 1) We do not know the factors that may control how far the thrust plate may ride over the surface before the reverse fault straightens itself by propagating through the hangingwall. This leads to abandonment of the section of the plate that overrode the land's surface; and 2) Material that is eroded off the front of the reverse scarp may be deformed by the advancing thrust plate or simply overridden. The controls on this process may be extremely site-specific. While a more physically reasonable representation of reverse fault scarps might include these factors, further field investigations that relate the rock physical properties, deformation rates, and thrust advance must be studied in detail.

The implicit assumption of the reinterpolation and normalization that is performed is that the effect of the horizontal strain is small relative to the vertical strain. Therefore, we expect our transport-limited approach to well- and poorly- approximate the topographic profile of the scarp when the fault dip is high and low, respectively. While these effects are ignored in this simple model, these avenues are fruitful paths of future research in fault scarp geomorphology.

Importantly, we have chosen an extremely simple system that consists of a single tectonic, geomorphic, and production process. Real scarps may be affected by many other production, transport and tectonic processes than those modeled. For example, channels, soil slips, bedrock landslides, debris flows [*e.g.*, Ritter *et al.*, 1995], and distributed deformation near the fault [Hilley *et al.*, 2001] are all processes that may act to create and modify topography around a fault. While this simple approach neglects them, it is a first step towards modeling more complex tectonic and geomorphic systems to understand fault scarp development.

Previous work [Arrowsmith *et al.*, 1996] reinterpolates the regolith/bedrock interface in the subsurface in addition to the topography at each time step. It has been shown [Hilley *et al.*, in review] that this type of interpolation does not allow the physically reasonable condition of bedrock and regolith juxtaposition in the subsurface. Reinterpolating this profile numerically erodes the bedrock, discouraging the onset of production-limited conditions. This situation arises purely as a model artifact, which once removed as in the current Penck1D model, allows fault movement to rapidly expose bedrock.

References

- Ahnert, F., Brief description of a comprehensive three-dimensional process-response model of landform development, *Z. Geomorphol. Suppl.*, 24 11–22, 1970.
- Anderson, R. S., and N. F. Humphrey, Interaction of weathering and transport processes in the evolution of arid landscapes, in *Quantitative Dynamic Stratigraphy*, edited by T. A. Cross, pp. 349–361, Prentice-Hall, Englewood Cliffs, N. J., 1989.
- Arrowsmith, J. R., *Coupled Tectonic Deformation and Geomorphic Degradation along the San Andreas Fault System*, Ph.D. dissertation, 356 pp., Stanford University, June 1995.
- Arrowsmith, J. R., D. D. Pollard, and D. D. Rhodes, Hillslope development in areas of active tectonics, *J. Geophys. Res.* 101, 6255–6275, 1996.
- Arrowsmith, J. R., D. D. Pollard, and D. D. Rhodes, Correction to “Hillslope development in areas of active tectonics,” *J. Geophys. Res.* 104 805, 1999a.
- Arrowsmith, J. R., Strecker, M. R., and Hilley, G. E., Holocene surface ruptures along the main Pamir Thrust in the Pamir-Alai region of southern Kyrgyzstan, *EOS Transactions AGU*, 80, 1016, 1999b.
- Avouac, J. P., Analysis of scarp profiles: evaluation of errors in morphologic dating, *Journal of Geophysical Research*, 98, 6745–6754, 1993.
- Carslaw, H. S., Jaeger, J. C., *Conduction of heat in solids*, 510 p., Oxford, Clarendon Press, 1959.
- Carson, M. A. and M. J. Kirkby, *Hillslope Form and Process*, 475 pp., Cambridge Univ. Press, New York, 1972.
- Chapra, S. C., P. C. Canale, *Numerical Methods for Engineers*, 812 p., McGraw-Hill, San Francisco, 1988.
- Culling, W. E. H., Analytical theory of erosion, *J. Geol.*, 68, 336–344, 1960.
- Davis, W. M., The convex profile of badland divides, *Science* 20, 245, 1892.
- Du, Y., P. Segall and H. Gao, Dislocations in inhomogeneous media via a moduli-perturbation approach: General formulation and two-dimensional solutions, *J. Geophys. Res.*, 99, 13,767–13,779, 1994.
- Fernandes, N., and W. E. Dietrich, Hillslope evolution by diffusive processes: the timescale for equilibrium adjustments, *Water Resources Res.* 33, 1307–1318, 1997.
- Ferziger, J. H., *Numerical Methods for Engineering Application*, 270 p., Wiley, New York, 1981.
- Gilbert, G. K., The convexity of hilltops, *J. Geol.* 17, 344–350, 1909.
- Hanks, T. C., The age of scarplike landforms from diffusion-equation analysis, in Noller, J. S., Sowers, J. M., and Lettis, W. R., eds., *Quaternary Geochronology*, AGU Reference Shelf, 4, 313–338, 2000.
- Hanks, T. C. and D. J. Andrews, Effect of far-field slope on morphologic dating of scarplike landforms, *Journal of Geophysical Research*, 94, 565–573, 1989.
- Hanks, T. C., R. C. Bucknam, K. R. Lajoie and R. E. Wallace, Modification of wave-cut and fault-controlled landforms, *Journal of Geophysical Research*, 89, 5771–5790, 1984.
- Heimsath, A. M., W. E. Dietrich, K. Nishiizumi, and R. C. Finkel, The soil production function and landscape equilibrium, *Nature* 388, 358–361, 1998.
- Heimsath, A. M., W. E. Dietrich, K. Nishiizumi, and R. C. Finkel, Cosmogenic nuclides, topography, and the spatial variation of soil depth, *Geomorphology*, 27, 151–172, 1999.

- Hilley, G. E., Arrowsmith, J. R., Amoroso, L., Interaction between normal faults and fractures and fault scarp morphology, *Geophys. Res. Lett.*, **28**, p. 3777–3780, 2001.
- Koons, P. O., The topographic evolution of collisional mountain belts; a numerical look at the Southern Alps, New Zealand, *Am. J. Sci.*, *289*, 1041–1069, 1989.
- Lave, J., and Avouac, J. P., Active folding of fluvial terraces across the Siwalik Hills, Himalayas of central Nepal, *J. Geophys. Res.*, *B*, *105*, 5735–5770, 2000.
- McCalpin, J., ed., *Paleoseismology*, 588 pp., Academic Press, San Diego, C. A., 1996.
- McKean, J. A., W. E. Dietrich, R. C. Finkel, J. R. Southon, and M. W. Caffee, Quantification of soil production and downslope creep rates from cosmogenic ^{10}Be accumulations on a hillslope profile, *Geology*, *21*, 343–346, 1993.
- Nash, D. B., Morphologic dating of degraded normal fault scarps, *J. Geol.* *88*, 353–360, 1980.
- Ritter, D. F., R. C. Kochel, J. R. Miller, *Process Geomorphology*, 546 p., Wm. C. Brown Publishers, Dubuque, I. A., 1995.
- Small, E. E., R. S. Anderson, and G. S. Hancock, Estimates of the rate of regolith production using ^{10}Be and ^{26}Al from an alpine hillslope, *Geomorphology* *27* 131–150, 1999.
- Stewart, I. S., P. L. Hancock, What is a fault scarp? *Episodes* *13*, 256–263, 1990.